Search for ultrarelativistic magnetic monopoles with the Pierre Auger observatory

A. Aab *et al.* (Pierre Auger Collaboration)

Search for Ultra-relativistic Magnetic Monopoles with the Pierre Auger Observatory

A. Aab,[1] P. Abreu,[2] M. Aglietta,[3,4] I. Al Samarai,[5] I.F.M. Albuquerque,[6] I. Allekotte,[7] A. Almela,[8,9] J. Alvarez Castillo,[10] J. Alvarez-Muñiz,[11] M. Ambrosio,[12] G.A. Anastasi,[13] L. Anchordoqui,[14] B. Andrada,[8] S. Andringa,[2] C. Aramo,[12] F. Arqueros,[15] N. Arsene,[16] H. Asorey,[7,17] P. Assis,[2] J. Aublin,[5] G. Avila,[18,19] A.M. Badescu,[20] A. Balaceanu,[21] R.J. Barreira Luz,[2] C. Baus,[22] J.J. Beatty,[23] K.H. Becker,[24] J.A. Bellido,[25] C. Berat,[26] M.E. Bertaina,[27,4] X. Bertou,[7] P.L. Biermann,[28] P. Billoir,[5] J. Biteau,[29] S.G. Blaess,[25] A. Blanco,[2] J. Blazek,[30] C. Bleve,[31,32] M. Boháčová,[30] D. Boncioli,[33,34] C. Bonifazi,[35] N. Borodai,[36] A.M. Botti,[8,37] J. Brack,[38] I. Brancus,[21] T. Bretz,[39] A. Bridgeman,[37] F.L. Briechle,[39] P. Buchholz,[1] A. Bueno,[40] S. Buitink,[41] M. Buscemi,[42,43] K.S. Caballero-Mora,[44] L. Caccianiga,[5] A. Cancio,[9,8] F. Canfora,[41] L. Caramete,[45] R. Caruso,[42,43] A. Castellina,[3,4] G. Cataldi,[32] L. Cazon,[2] R. Cester,[27,4] A.G. Chavez,[46] J.A. Chinellato,[47] J. Chudoba,[30] R.W. Clay,[25] R. Colalillo,[48,12] A. Coleman,[49] L. Collica,[4] M.R. Coluccia,[31,32] R. Conceição,[2] F. Contreras,[18,19] M.J. Cooper,[25] S. Coutu,[49] C.E. Covault,[50] J. Cronin,[51] S. D'Amico,[52,32] B. Daniel,[47] S. Dasso,[53,54] K. Daumiller,[37] B.R. Dawson,[25] R.M. de Almeida,[55] S.J. de Jong,[41,56] G. De Mauro,[41] J.R.T. de Mello Neto,[35] I. De Mitri,[31,32] J. de Oliveira,[55] V. de Souza,[57] J. Debatin,[37] O. Deligny,[29] C. Di Giulio,[58,59] A. Di Matteo,[60,61] M.L. Díaz Castro,[47] F. Diogo,[2] C. Dobrigkeit,[47] J.C. D'Olivo,[10] A. Dorofeev,[38] R.C. dos Anjos,[62] M.T. Dova,[63] A. Dundovic,[64] J. Ebr,[30] R. Engel,[37] M. Erdmann,[39] M. Erfani,[1] C.O. Escobar,[65,47] J. Espadanal,[2] A. Etchegoyen,[8,9] H. Falcke,[41,66,56] K. Fang,[51] G. Farrar,[67] A.C. Fauth,[47] N. Fazzini,[65] B. Fick,[68] J.M. Figueira,[8] A. Filipčič,[69,70] O. Fratu,[20] M.M. Freire,[71] T. Fujii,[51] A. Fuster,[8,9] R. Gaior,[5] B. García,[72] D. Garcia-Pinto,[15] F. Gaté,[73] H. Gemmeke,[73] A. Gherghel-Lascu,[21] P.L. Ghia,[5] U. Giaccari,[35] M. Giammarchi,[74] M. Giller,[75] D. Głas,[76] C. Glaser,[39] H. Glass,[65] G. Golup,[7] M. Gómez Berisso,[7] P.F. Gómez Vitale,[18,19] N. González,[8,37] B. Gookin,[38] A. Gorgi,[3,4] P. Gorham,[77] P. Gouffon,[6] A.F. Grillo,[33] T.D. Grubb,[25] F. Guarino,[48,12] G.P. Guedes,[78] M.R. Hampel,[8] P. Hansen,[63] D. Harari,[7] T.A. Harrison,[25] J.L. Harton,[38] Q. Hasankiadeh,[79] A. Haungs,[37] T. Hebbeker,[39] D. Heck,[37] P. Heimann,[1] A.E. Herve,[22] G.C. Hill,[25] C. Hojvat,[65] E. Holt,[37,8] P. Homola,[36] J.R. Hörandel,[41,56] P. Horvath,[80] M. Hrabovský,[80] T. Huege,[37] J. Hulsman,[8,37] A. Insolia,[42,43] P.G. Isar,[45] I. Jandt,[24] S. Jansen,[41,56] J.A. Johnsen,[81] M. Josebachuili,[8] A. Kääpä,[24] O. Kambeitz,[22] K.H. Kampert,[24] P. Kasper,[65] I. Katkov,[22] B. Keilhauer,[37] E. Kemp,[47] J. Kemp,[39] R.M. Kieckhafer,[68] H.O. Klages,[37] M. Kleifges,[73] J. Kleinfeller,[18] R. Krause,[39] N. Krohm,[24] D. Kuempel,[39] G. Kukec Mezek,[70] N. Kunka,[73] A. Kuotb Awad,[37] D. LaHurd,[50] M. Lauscher,[39] P. Lebrun,[65] R. Legumina,[75] M.A. Leigui de Oliveira,[82] A. Letessier-Selvon,[5] I. Lhenry-Yvon,[29] K. Link,[22] L. Lopes,[2] R. López,[83] A. López Casado,[11] Q. Luce,[29] A. Lucero,[8,9] M. Malacari,[51] M. Mallamaci,[84,74] D. Mandat,[30] P. Mantsch,[65] A.G. Mariazzi,[63] I.C. Mariş,[40] G. Marsella,[31,32] D. Martello,[31,32] H. Martinez,[85] O. Martínez Bravo,[83] J.J. Masías Meza,[54] H.J. Mathes,[37] S. Mathys,[24] J. Matthews,[86] J.A.J. Matthews,[87] G. Matthiae,[58,59] E. Mayotte,[24] P.O. Mazur,[65] C. Medina,[81] G. Medina-Tanco,[10] D. Melo,[8] A. Menshikov,[73] S. Messina,[79] M.I. Micheletti,[71] L. Middendorf,[39] I.A. Minaya,[15] L. Miramonti,[84,74] B. Mitrica,[21] D. Mockler,[22] L. Molina-Bueno,[40] F. Montanet,[26] C. Morello,[3,4] M. Mostafá,[49] G. Müller,[39] M.A. Muller,[47,88] S. Müller,[37,8] I. Naranjo,[7] L. Nellen,[10] J. Neuser,[24] P.H. Nguyen,[25] M. Niculescu-Oglinzanu,[21] M. Niechciol,[1] L. Niemietz,[24] T. Niggemann,[39] D. Nitz,[68] D. Nosek,[89] V. Novotny,[89] H. Nožka,[80] L.A. Núñez,[17] L. Ochilo,[1] F. Oikonomou,[49] A. Olinto,[51] D. Pakk Selmi-Dei,[47] M. Palatka,[30] J. Pallotta,[90] P. Papenbreer,[24] G. Parente,[11] A. Parra,[83] T. Paul,[91,14] M. Pech,[30] F. Pedreira,[11] J. Pękala,[36] R. Pelayo,[92] J. Peña-Rodriguez,[17] L. A. S. Pereira,[47] L. Perrone,[31,32] C. Peters,[39] S. Petrera,[60,13,61] J. Phuntsok,[49] R. Piegaia,[54] T. Pierog,[37] P. Pieroni,[54] M. Pimenta,[2] V. Pirronello,[42,43] M. Platino,[8] M. Plum,[39] C. Porowski,[36] R.R. Prado,[57] P. Privitera,[51] M. Prouza,[30] E.J. Quel,[90] S. Querchfeld,[24] S. Quinn,[50] R. Ramos-Pollan,[17] J. Rautenberg,[24] D. Ravignani,[8] D. Reinert,[39] B. Revenu,[93] J. Ridky,[30] M. Risse,[1] P. Ristori,[90] V. Rizi,[60,61] W. Rodrigues de Carvalho,[6] G. Rodriguez Fernandez,[58,59] J. Rodriguez Rojo,[18] D. Rogozin,[37] M. Roth,[37] E. Roulet,[7] A.C. Rovero,[53] S.J. Saffi,[25] A. Saftoiu,[21] F. Salamida,[29,94] H. Salazar,[83] A. Saleh,[70] F. Salesa Greus,[49] G. Salina,[59] J.D. Sanabria Gomez,[17] F. Sánchez,[8] P. Sanchez-Lucas,[40] E.M. Santos,[6] E. Santos,[8] F. Sarazin,[81] B. Sarkar,[24] R. Sarmento,[2] C.A. Sarmiento,[8] R. Sato,[18] M. Schauer,[24] V. Scherini,[31,32] H. Schieler,[37] M. Schimp,[24] D. Schmidt,[37,8] O. Scholten,[79,95] P. Schovánek,[30] F.G. Schröder,[37] A. Schulz,[37] J. Schulz,[41] J. Schumacher,[39] S.J. Sciutto,[63] A. Segreto,[96,43] M. Settimo,[5] A. Shadkam,[86] R.C. Shellard,[97] G. Sigl,[64] G. Silli,[8,37] O. Sima,[16] A. Śmiałkowski,[75] R. Šmída,[37] G.R. Snow,[98] P. Sommers,[49] S. Sonntag,[1] J. Sorokin,[25] R. Squartini,[18] D. Stanca,[21] S. Stanič,[70] J. Stasielak,[36] P. Stassi,[26] F. Strafella,[31,32] F. Suarez,[8,9] M. Suarez Durán,[17] T. Sudholz,[25] T. Suomijärvi,[29] A.D. Supanitsky,[53] J. Swain,[91] Z. Szadkowski,[76] A. Taboada,[22] O.A. Taborda,[7] A. Tapia,[8] V.M. Theodoro,[47] C. Timmermans,[56,41] C.J. Todero Peixoto,[99] L. Tomankova,[37] B. Tomé,[2] G. Torralba Elipe,[11] D. Torres Machado,[35] M. Torri,[84] P. Travnicek,[30] M. Trini,[70] R. Ulrich,[37] M. Unger,[67,37] M. Urban,[39] J.F. Valdés Galicia,[10] I. Valiño,[11] L. Valore,[48,12] G. van Aar,[41] P. van Bodegom,[25] A.M. van den Berg,[79] A. van

Vliet,[41] E. Varela,[83] B. Vargas Cárdenas,[10] G. Varner,[77] J.R. Vázquez,[15] R.A. Vázquez,[11] D. Veberič,[37]
I.D. Vergara Quispe,[63] V. Verzi,[59] J. Vicha,[30] L. Villaseñor,[46] S. Vorobiov,[70] H. Wahlberg,[63] O. Wainberg,[8, 9]
D. Walz,[39] A.A. Watson,[100] M. Weber,[73] A. Weindl,[37] L. Wiencke,[81] H. Wilczyński,[36] T. Winchen,[24]
D. Wittkowski,[24] B. Wundheiler,[8] S. Wykes,[41] L. Yang,[70] D. Yelos,[9, 8] A. Yushkov,[8] E. Zas,[11] D. Zavrtanik,[70, 69]
M. Zavrtanik,[69, 70] A. Zepeda,[85] B. Zimmermann,[73] M. Ziolkowski,[1] Z. Zong,[29] and F. Zuccarello[42, 43]

(The Pierre Auger Collaboration)[, *]

[1]*Universität Siegen, Fachbereich 7 Physik – Experimentelle Teilchenphysik, Germany*
[2]*Laboratório de Instrumentação e Física Experimental de Partículas – LIP*
and Instituto Superior Técnico – IST, Universidade de Lisboa – UL, Portugal
[3]*Osservatorio Astrofisico di Torino (INAF), Torino, Italy*
[4]*INFN, Sezione di Torino, Italy*
[5]*Laboratoire de Physique Nucléaire et de Hautes Energies (LPNHE),*
Universités Paris 6 et Paris 7, CNRS-IN2P3, France
[6]*Universidade de São Paulo, Inst. de Física, São Paulo, Brazil*
[7]*Centro Atómico Bariloche and Instituto Balseiro (CNEA-UNCuyo-CONICET), Argentina*
[8]*Instituto de Tecnologías en Detección y Astropartículas (CNEA,*
CONICET, UNSAM), Centro Atómico Constituyentes,
Comisión Nacional de Energía Atómica, Argentina
[9]*Universidad Tecnológica Nacional – Facultad Regional Buenos Aires, Argentina*
[10]*Universidad Nacional Autónoma de México, México*
[11]*Universidad de Santiago de Compostela, Spain*
[12]*INFN, Sezione di Napoli, Italy*
[13]*Gran Sasso Science Institute (INFN), L'Aquila, Italy*
[14]*Department of Physics and Astronomy, Lehman College, City University of New York, USA*
[15]*Universidad Complutense de Madrid, Spain*
[16]*University of Bucharest, Physics Department, Romania*
[17]*Universidad Industrial de Santander, Colombia*
[18]*Observatorio Pierre Auger, Argentina*
[19]*Observatorio Pierre Auger and Comisión Nacional de Energía Atómica, Argentina*
[20]*University Politehnica of Bucharest, Romania*
[21]*"Horia Hulubei" National Institute for Physics and Nuclear Engineering, Romania*
[22]*Karlsruhe Institute of Technology, Institut für Experimentelle Kernphysik (IEKP), Germany*
[23]*Ohio State University, USA*
[24]*Bergische Universität Wuppertal, Department of Physics, Germany*
[25]*University of Adelaide, Australia*
[26]*Laboratoire de Physique Subatomique et de Cosmologie (LPSC),*
Université Grenoble-Alpes, CNRS/IN2P3, France
[27]*Università Torino, Dipartimento di Fisica, Italy*
[28]*Max-Planck-Institut für Radioastronomie, Bonn, Germany*
[29]*Institut de Physique Nucléaire d'Orsay (IPNO), Université Paris 11, CNRS-IN2P3, France*
[30]*Institute of Physics (FZU) of the Academy of Sciences of the Czech Republic, Czech Republic*
[31]*Università del Salento, Dipartimento di Matematica e Fisica "E. De Giorgi", Italy*
[32]*INFN, Sezione di Lecce, Italy*
[33]*INFN Laboratori Nazionali del Gran Sasso, Italy*
[34]*now at Deutsches Elektronen-Synchrotron (DESY), Zeuthen, Germany*
[35]*Universidade Federal do Rio de Janeiro (UFRJ), Instituto de Física, Brazil*
[36]*Institute of Nuclear Physics PAN, Poland*
[37]*Karlsruhe Institute of Technology, Institut für Kernphysik (IKP), Germany*
[38]*Colorado State University, USA*
[39]*RWTH Aachen University, III. Physikalisches Institut A, Germany*
[40]*Universidad de Granada and C.A.F.P.E., Spain*
[41]*Institute for Mathematics, Astrophysics and Particle Physics (IMAPP), Radboud Universiteit, Nijmegen, Netherlands*
[42]*Università di Catania, Dipartimento di Fisica e Astronomia, Italy*
[43]*INFN, Sezione di Catania, Italy*
[44]*Universidad Autónoma de Chiapas, México*
[45]*Institute of Space Science, Romania*
[46]*Universidad Michoacana de San Nicolás de Hidalgo, México*
[47]*Universidade Estadual de Campinas (UNICAMP), Brazil*
[48]*Università di Napoli "Federico II", Dipartimento di Fisica "Ettore Pancini", Italy*
[49]*Pennsylvania State University, USA*
[50]*Case Western Reserve University, USA*
[51]*University of Chicago, USA*

[52] Università del Salento, Dipartimento di Ingegneria, Italy

[53] Instituto de Astronomía y Física del Espacio (IAFE, CONICET-UBA), Argentina

[54] Departamento de Física and Departamento de Ciencias de la Atmósfera y los Océanos, FCEyN, Universidad de Buenos Aires, Argentina

[55] Universidade Federal Fluminense, Brazil

[56] Nationaal Instituut voor Kernfysica en Hoge Energie Fysica (NIKHEF), Netherlands

[57] Universidade de São Paulo, Inst. de Física de São Carlos, São Carlos, Brazil

[58] Università di Roma "Tor Vergata", Dipartimento di Fisica, Italy

[59] INFN, Sezione di Roma "Tor Vergata", Italy

[60] Università dell'Aquila, Dipartimento di Scienze Fisiche e Chimiche, Italy

[61] INFN, Gruppo Collegato dell'Aquila, Italy

[62] Universidade Federal do Paraná, Setor Palotina, Brazil

[63] IFLP, Universidad Nacional de La Plata and CONICET, Argentina

[64] Universität Hamburg, II. Institut für Theoretische Physik, Germany

[65] Fermi National Accelerator Laboratory, USA

[66] Stichting Astronomisch Onderzoek in Nederland (ASTRON), Dwingeloo, Netherlands

[67] New York University, USA

[68] Michigan Technological University, USA

[69] Experimental Particle Physics Department, J. Stefan Institute, Slovenia

[70] Laboratory for Astroparticle Physics, University of Nova Gorica, Slovenia

[71] Instituto de Física de Rosario (IFIR) – CONICET/U.N.R. and Facultad de Ciencias Bioquímicas y Farmacéuticas U.N.R., Argentina

[72] Instituto de Tecnologías en Detección y Astropartículas (CNEA, CONICET, UNSAM) and Universidad Tecnológica Nacional – Facultad Regional Mendoza (CONICET/CNEA), Argentina

[73] Karlsruhe Institute of Technology, Institut für Prozessdatenverarbeitung und Elektronik (IPE), Germany

[74] INFN, Sezione di Milano, Italy

[75] University of Łódź, Faculty of Astrophysics, Poland

[76] University of Łódź, Faculty of High-Energy Astrophysics, Poland

[77] University of Hawaii, USA

[78] Universidade Estadual de Feira de Santana (UEFS), Brazil

[79] KVI – Center for Advanced Radiation Technology, University of Groningen, Netherlands

[80] Palacky University, RCPTM, Czech Republic

[81] Colorado School of Mines, USA

[82] Universidade Federal do ABC (UFABC), Brazil

[83] Benemérita Universidad Autónoma de Puebla (BUAP), México

[84] Università di Milano, Dipartimento di Fisica, Italy

[85] Centro de Investigación y de Estudios Avanzados del IPN (CINVESTAV), México

[86] Louisiana State University, USA

[87] University of New Mexico, USA

[88] Universidade Federal de Pelotas, Brazil

[89] University Prague, Institute of Particle and Nuclear Physics, Czech Republic

[90] Centro de Investigaciones en Láseres y Aplicaciones, CITEDEF and CONICET, Argentina

[91] Northeastern University, USA

[92] Unidad Profesional Interdisciplinaria en Ingeniería y Tecnologías Avanzadas del Instituto Politécnico Nacional (UPIITA-IPN), México

[93] SUBATECH, École des Mines de Nantes, CNRS-IN2P3, Université de Nantes

[94] INFN, Sezione di Milano Bicocca, Italy

[95] also at Vrije Universiteit Brussels, Brussels, Belgium

[96] INAF – Istituto di Astrofisica Spaziale e Fisica Cosmica di Palermo, Italy

[97] Centro Brasileiro de Pesquisas Fisicas (CBPF), Brazil

[98] University of Nebraska, USA

[99] Universidade de São Paulo, Escola de Engenharia de Lorena, Brazil

[100] School of Physics and Astronomy, University of Leeds, Leeds, United Kingdom

We present a search for ultra-relativistic magnetic monopoles with the Pierre Auger Observatory. Such particles, possibly a relic of phase transitions in the early universe, would deposit a large amount of energy along their path through the atmosphere, comparable to that of ultrahigh-energy cosmic rays (UHECRs). The air shower profile of a magnetic monopole can be effectively distinguished by the fluorescence detector from that of standard UHECRs. No candidate was found in the data collected between 2004 and 2012, with an expected background of less than 0.1 event from UHECRs. The corresponding 90% confidence level (C.L.) upper limits on the flux of ultra-relativistic magnetic monopoles range from 10^{-19} (cm^2 sr s)$^{-1}$ for a Lorentz factor $\gamma = 10^9$ to 2.5×10^{-21} (cm^2 sr s)$^{-1}$ for $\gamma = 10^{12}$. These results - the first obtained with a UHECR detector - improve previously published limits by up to an order of magnitude.

I. INTRODUCTION

Maxwell's unified description of electric and magnetic phenomena is one of the greatest achievements of 19th century physics. Free magnetic charges and currents are not allowed in Maxwell's equations, a consequence of their apparent absence in Nature. On the other hand, there are essential theoretical motivations for magnetic monopoles. Their existence would naturally explain the quantization of electric charge, as first noted by Dirac [1] in 1931. Also, magnetic monopoles are required in Grand Unified Theories (GUTs), where they appear as intrinsically stable topological defects when a symmetry breaking results in a U(1) subgroup [2–4]. In typical GUT models, supermassive magnetic monopoles ($M \approx 10^{26}$ eV/c^2) are produced in the early Universe at the phase transition corresponding to the spontaneous symmetry breaking of the unified fundamental interactions. When the original unified group undergoes secondary symmetry breaking at lower energy scales, so-called intermediate-mass monopoles (IMMs, $M \sim 10^{11} - 10^{20}$ eV/c^2) may be generated. These particles, too massive to be produced at accelerators, may be present today as a cosmic-radiation relic of such early Universe transitions.

Supermassive magnetic monopoles should be gravitationally bound to the Galaxy (or to the Sun or Earth) with non-relativistic virial velocities [2–4]. Lighter magnetic monopoles can reach relativistic velocities through acceleration in coherent domains of the Galactic and intergalactic magnetic fields, as well as in astrophysical objects (e.g., neutron stars) [5, 6]. Kinetic energies of the order of 10^{25} eV have been predicted [7], which result in ultra-relativistic velocities for IMMs. Large-exposure experimental searches for magnetic monopoles are based on their velocity-dependent interactions with matter, with a wide range of velocities allowed for GUT monopoles.

There is a long history of experimental searches for magnetic monopoles with a variety of experiments such as MACRO [8], AMANDA [9], Baikal [10], SLIM [11], RICE [12], ANITA [13] and IceCube [14]. The strongest upper limit on the flux of non-relativistic magnetic monopoles ($4 \times 10^{-5} < \beta = v/c < 0.5$) comes from the MACRO experiment at $\approx 1.5 \times 10^{-16}$ (cm^2 sr s)$^{-1}$ (90% C.L.) [8]. At relativistic velocities ($\beta \approx 0.9$), the IceCube Observatory has placed the best limit at $\approx 4 \times 10^{-18}$ (cm^2 sr s)$^{-1}$ [14]. The best limit on the flux of ultra-relativistic IMMs (Lorentz factor $\gamma \approx 10^{11}$) is reported by the ANITA-II experiment at $\approx 10^{-19}$ (cm^2 sr s)$^{-1}$ [13].

These upper limits are below the Parker bound [15] of $\sim 10^{-15}$ (cm^2 sr s)$^{-1}$, which represents the largest possible magnetic-monopole flux consistent with survival of the Galactic magnetic field. However, the original Parker bound does not take into account the current knowledge of the Galactic magnetic field and its almost chaotic nature, with domain lengths in the range $1 - 10$ kpc. The so-called "extended Parker bound" [16] becomes mass-dependent with $\Phi \sim 10^{-16} M/(10^{26}$ eV$)$ (cm^2 sr s)$^{-1}$ with M the monopole mass, and is well below current experimental sensitivities (for relativistic and ultra-relativistic monopoles).

In this paper, we report a search for ultra-relativistic IMMs with data collected with the Pierre Auger Observatory between 1 December 2004 and 31 December 2012. Details of the Observatory are given in Section II. The search is motivated by the large energy deposited by ultra-relativistic IMMs along their path in the atmosphere, comparable to that of UHECRs, with a distinctive longitudinal development well-suited for detection by the fluorescence detector. The characteristics of air showers induced by IMMs are described in Section III. Simulations and event reconstruction procedures are presented in Section IV. The event selection criteria are described in Section V. The exposure, i.e., the time-integrated aperture, for the IMM search is evaluated in Section VI. Details of the data analysis and results are presented in Section VII. Conclusions are drawn in Section VIII.

II. PIERRE AUGER OBSERVATORY

The Pierre Auger Observatory [17] is the largest UHECR detector currently in operation. Located in the southern hemisphere in western Argentina, just northeast of the town of Malargüe (69°W, 35°S, 1400 m a.s.l.), it covers an area of 3000 km^2 with a surface-detector array (SD) [18] overlooked by a fluorescence detector (FD) [19].

The SD consists of 1660 water-Cherenkov detectors arranged in a triangular grid of 1500 m spacing, operating with a duty cycle of nearly 100%. The SD stations detect at ground level the secondary particles of the extensive air shower (EAS) produced by the UHECR primary interaction in the atmosphere. The FD detects the UV fluorescence light from nitrogen molecules excited by the EAS particles along their path in the atmosphere. Its operation is limited to clear moonless nights, resulting in a duty cycle of $\sim 15\%$ [17]. The FD consists of 24 telescopes, arranged in groups of six at four sites overlooking the SD. Each telescope has a field of view of 30° × 30° in azimuth and elevation, with a 13 m^2 spherical segmented mirror collecting fluorescence light onto a 440 photomultiplier (PMT) camera. The telescope's 3.8 m^2 aperture optics are of the Schmidt design and are equipped with

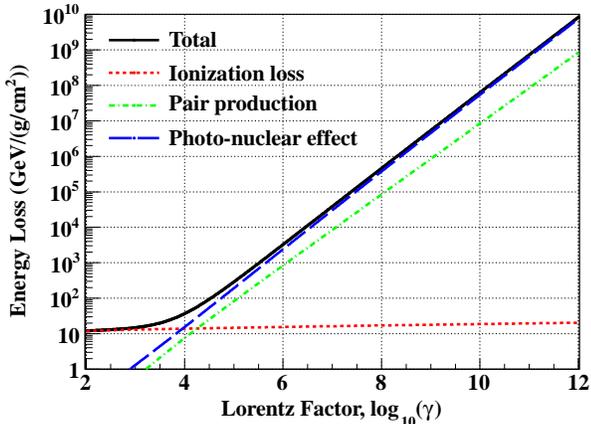*Electronic address: auger_spokespersons@fnal.gov; URL: http://www.auger.org

FIG. 1: Energy loss of a magnetic monopole in air as a function of its Lorentz factor γ.

an annular corrector lens to minimize spherical aberration. The FD measures the longitudinal development of the UHECR shower in the atmosphere, since the fluorescence light is proportional to the energy deposited by the EAS particles [20–22]. The depth corresponding to the maximum energy deposit, $X_{\max}$, and a calorimetric estimate of the shower energy are obtained from a fit of the shower profile. For the present analysis, we will use "hybrid" events - showers simultaneously detected by the FD and SD - which are reconstructed with superior resolution: $\sim 0.6°$ in arrival direction, $\sim 6\%$ in energy and ≤ 20 g/cm^2 in $X_{\max}$, respectively [23]. Systematic uncertainties on the energy and $X_{\max}$ are 14% [17, 24] and ≤ 10 g/cm^2 [23], respectively.

III. ULTRA-RELATIVISTIC MONOPOLE-INDUCED AIR SHOWERS

Electromagnetic interactions of magnetic monopoles have been extensively investigated [7, 25]. The electromagnetic energy loss of a magnetic monopole in air is shown in Figure 1 as a function of its Lorentz factor $\gamma = E_{\mathrm{mon}}/M$. Collisional energy loss is the dominant contribution for $\gamma \leq 10^4$. At higher Lorentz factors, pair production and photo-nuclear interactions become the main cause of energy loss. Bremsstrahlung is highly suppressed by the large monopole mass. An ultra-relativistic IMM would deposit a large amount of energy in its passage through the Earth's atmosphere, comparable to that of a UHECR. For example, a singly-charged IMM with $\gamma = 10^{11}$ loses ≈ 700 PeV/(g/cm^2) (cf. Figure 1), which sums up to $\approx 10^{20.8}$ eV when integrated over an atmospheric depth of ≈ 1000 g/cm^2. This energy will be dissipated by the IMM through production of secondary showers initiated by photo-nuclear effects and pair productions along its path.

In order to study the characteristics of IMM-induced showers, we implemented magnetic-monopole interactions in the CORSIKA air-shower simulation software [26]. Specifically, existing subroutines for muonic collisional loss, e^+e^--pair production and photo-nuclear interaction were appropriately modified in CONEX [27], which can be used within CORSIKA to perform a combination of stochastic particle production and numeric integration of particle cascades. We used [28, 29] to parameterize the differential cross section for e^+e^--pair production and the Bezrukov-Bugaev parameterization [30, 31] for the photo-nuclear interaction model. To describe magnetic monopole interactions, the cross sections were scaled up by a factor z_M^2 [7, 25], where $z_M = 1/(2\alpha)$ is the singly-charged monopole charge and α is the fine-structure constant. Pair production and photo-nuclear interactions were treated explicitly as stochastic processes resulting in secondary particles produced along the monopole path in the atmosphere. Standard CONEX routines were used to simulate showers originating from these secondary particles. Collisional losses were implemented as continuous energy losses.
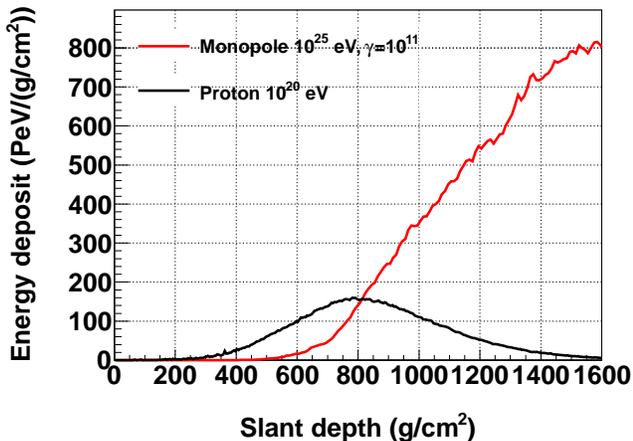
The longitudinal profile of the energy deposited by an ultra-relativistic IMM of $E_{\mathrm{mon}} = 10^{25}$ eV, $\gamma = 10^{11}$ and zenith angle of 70° is shown in Figure 2. When compared with a standard UHECR proton shower of energy 10^{20} eV (black solid line in Figure 2), the IMM shower presents a much larger energy deposit and deeper development, due to the superposition of many showers uniformly produced by the IMM along its path in the atmosphere. This distinctive feature will be used in our analysis, which is based on the shower development measured in the hybrid events. Also, we have confirmed this feature in case if we use other parameterizations (e.g., ALLM [32]), meaning the difference between cross sections is a second order effect for the shower profile of IMM. Depending on their energy, ultra-relativistic IMMs may traverse the Earth [13, 14] and emerge from the ground producing upward-going showers. We have not searched for this kind of candidate, which would not guarantee a high-quality reconstruction of the shower development.

IV. MONTE CARLO SIMULATIONS AND EVENT RECONSTRUCTION

Monte Carlo samples of ultra-relativistic IMMs were simulated for Lorentz factors in the range $\gamma = 10^8 - 10^{12}$ at a fixed monopole energy of $E_{\mathrm{mon}} = 10^{25}$ eV, because the monopole energy loss does not depend on E_{mon} but rather on γ in the ultra-relativistic regime of this search. While we used a fixed E_{mon} in the simulations, the results can be readily applied to a much larger range of monopole energies.

To estimate the background from UHECRs, we simulated proton showers with energy E_{p} between 10^{18} eV and 10^{21} eV. Proton primaries are chosen to obtain a conservative estimate of the cosmic-ray background (cf.

FIG. 2: Longitudinal profile of the energy deposited by an ultra-relativistic IMM of $E_{\mathrm{mon}} = 10^{25}$ eV, $\gamma = 10^{11}$ and zenith angle of $70°$ (red solid line). The profile of a UHECR proton shower of energy 10^{20} eV is shown as a black solid line.

Sec. VII). We used three different models - QGSJetII-04, Sibyll 2.1 and EPOS-LHC - to account for uncertainties in the hadronic interactions. Events were simulated according to an E_{p}^{-1} energy spectrum, to ensure sufficient Monte Carlo statistics at the highest energy, and then appropriately weighted to reproduce the energy spectrum measured by the Pierre Auger Observatory [33].

For both the IMM and UHECR simulations, we used the CORSIKA package [26] to generate an isotropic distribution of showers above the horizon, and the Auger Offline software [34] to produce the corresponding FD and SD events. We found that the standard event reconstruction, which is optimized for UHECRs, provides equally accurate direction and longitudinal profile for ultra-relativistic IMM showers. An example of reconstructed longitudinal profile for a simulated magnetic monopole of energy 10^{25} eV and $\gamma = 10^{11}$ is shown in Figure 3 indicating the profile of the generated COR-SIKA shower (blue line) and the result of a fit of the reconstructed profile with a Gaisser-Hillas function [35] (red line). For standard UHECRs, the energy, E_{sh}, and the depth of maximum development, X_{max}, of the shower are estimated by the integral of the fitted profile and by the position of its maximum, respectively. When applied to an ultra-relativistic IMM shower profile, the Gaisser-Hillas parameterization provides a very good fit of the portion of the profile detected in the FD field of view (cf. red and blue lines in Figure 3 in the relevant range). Also, due to the steep rising of the ultra-relativistic IMM profile, the fit systematically converges to a value of X_{max} beyond the lower edge of the FD field of view, corresponding to the largest visible slant depth, X_{up}. We will use this characteristic to reject most of the standard UHECR showers, which constitute the background for this search. Since X_{max} of standard UHECR showers are located in
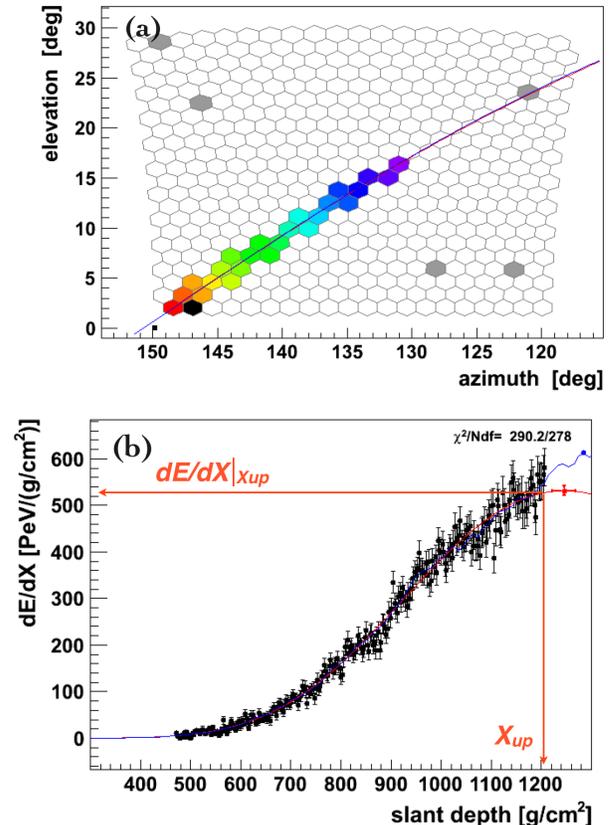
FIG. 3: Reconstructed signals for a simulated magnetic monopole of energy 10^{25} eV and $\gamma = 10^{11}$. In (a), the FD camera view is shown with color-coded timing of triggered pixels (time increases from blue to red). The red (blue) line indicates the reconstructed (simulated) shower direction projected on the camera view. In (b), the reconstructed longitudinal profile of the shower is shown. The red line is the result of a Gaisser-Hillas fit of the profile, with the red cross indicating the position of X_{max}. The blue line represents the simulated profile of the monopole shower. The selection variables X_{up}, the largest visible slant depth, and $dE/dX|_{X\mathrm{up}}$, energy deposited at X_{up}, are also indicated.

FD field of view, a specific selection is required to search for the IMM profile.

V. EVENT SELECTION

We restricted our event selection to time periods with good operating conditions of the FD telescopes and well-defined calibration constants. Additional requirements were imposed on the quality of the atmosphere (aerosols and cloud coverage). Details on these data-quality criteria can be found in [23]. A total of 376,084 hybrid shower candidates were selected.

A further set of selection criteria was applied to ensure good-quality showers. We required the zenith angle of the shower to be $< 60°$, and the distance of the

shower core to the SD station with the highest signal to be less than 1500 m. The shower must be seen by at least five FD pixels over a slant depth interval of at least 200 g/cm^2. We rejected events with gaps in their profile of more than 20% of the profile length, which could be due to telescope-border effects. The Gaisser-Hillas fit of the shower profile was required to have a $\chi^2/\mathrm{ndf} < 2.5$, where ndf is the number of degrees of freedom. To guarantee full SD-trigger efficiency, the shower must have a minimum energy. Rather than using E_{sh}, which is ill-defined for an ultra-relativistic IMM shower, we employed the energy deposited at the largest visible slant depth X_{up}, $dE/dX|_{X\mathrm{up}}$, as a discriminating variable related to the shower energy (Figure 3). The $dE/dX|_{X\mathrm{up}}$ is calculated by the result of the Gaisser-Hillas fit. The requirement $dE/dX|_{X\mathrm{up}} > 3.0$ PeV/(g/cm^2) is equivalent to an energy threshold of $\approx 10^{18.5}$ eV, where the SD is fully efficient. These shower-quality criteria selected a sample of well-reconstructed events, and are efficient for UHECRs as well as ultra-relativistic IMM showers.

Additional criteria for IMM selection were established from Monte Carlo simulations described in Section IV. We required X_{max} to be larger than X_{up}, which is almost always fulfilled by ultra-relativistic IMM showers. Only 6% of the UHECR proton showers of $10^{18.5}$ eV survived this cut, the fraction increasing to 32% for $10^{20.5}$ eV showers. A further reduction was obtained by appropriate constraints on the penetration of the shower and its energy deposit. To illustrate this second requirement, we show in Figure 4(a) the correlation of $dE/dX|_{X\mathrm{up}}$ with X_{up} for UHECR background events passing the shower-quality criteria. When $X_{\mathrm{max}} > X_{\mathrm{up}}$ is required, the number of events is drastically reduced and the population becomes constrained in a much smaller region, as shown in Figure 4(b). The maximum value of X_{max} found in the UHECR proton simulated events is ≈ 1100 g/cm^2, which results in the X_{up} upper boundary of Figure 4(b): X_{max} is always in the FD field of view when $X_{\mathrm{up}} \gtrsim 1100$ g/cm^2. On the other hand, the reconstructed X_{max} will always be outside the FD field of view for ultra-relativistic IMM showers, independently of the shower's X_{up}. This is apparent in Figure 5, where the correlation of $dE/dX|_{X\mathrm{up}}$ with X_{up} is shown for ultra-relativistic IMM simulated events. The background from UHECRs is almost eliminated by excluding an appropriate region of the $(X_{\mathrm{up}}, dE/dX|_{X\mathrm{up}})$ plane. We optimized the selection to achieve less than 0.1 background event expected in the data set of this search. The final requirement, $X_{\mathrm{up}} > 1080$ g/cm^2 or $dE/dX|_{X\mathrm{up}} > 150$ PeV/(g/cm^2), is shown in Figure 4(b) and Figure 5 as dashed boxes, and results in an expected background of 0.07 event in the search-period data set.

The selection criteria used for this search are summarized in Table I. The corresponding selection efficiency for ultra-relativistic IMMs ranges from 3% for $\gamma = 10^9$ to 91% for $\gamma = 10^{12}$ (see Table II).
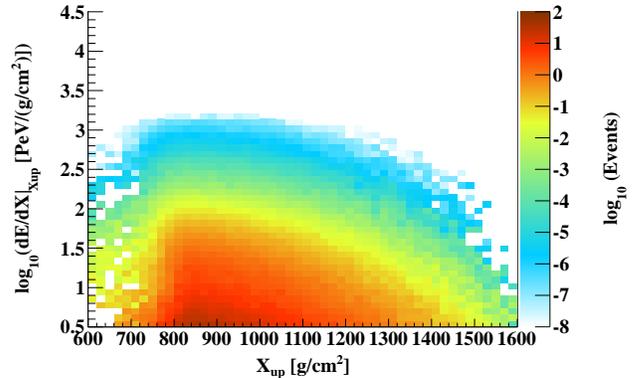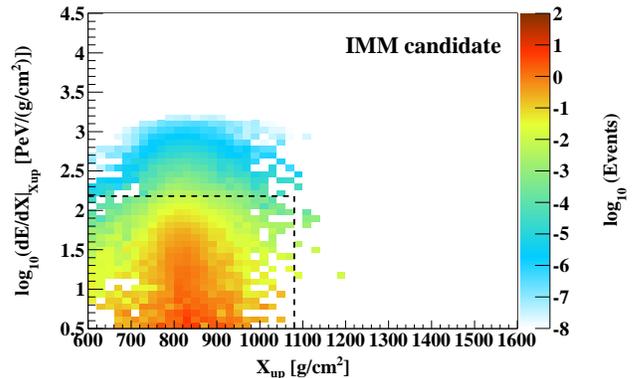

(a)Shower quality selection

(b)$X_{\mathrm{max}} > X_{\mathrm{up}}$ selection

FIG. 4: Correlation of $dE/dX|_{X\mathrm{up}}$ with X_{up} for simulated UHECR proton showers passing the quality-selection criteria (a) and the additional requirement $X_{\mathrm{max}} > X_{\mathrm{up}}$ (b). The color-coded scale indicates the number of events expected in the search-period data set based on the energy spectrum measured with Auger [33]. Only events outside the dashed box in (b) are kept in the final selection for ultra-relativistic IMMs.

Shower-quality selection criteria	#events	$f(\%)$
Reconstructed events	376,084	—
Zenith angle $< 60°$	360,159	95.8
Distance from nearest SD < 1500 m	359,467	99.8
Number of FD pixels > 5	321,293	89.4
Slant-depth interval > 200 g/cm^2	205,165	63.9
Gaps in profile $< 20\%$	199,625	97.3
profile fit $\chi^2/\mathrm{ndf} < 2.5$	197,293	98.8
$dE/dX|_{X\mathrm{up}} > 3.0$ PeV/(g/cm^2)	6812	3.5
Magnetic-monopole selection criteria		
$X_{\mathrm{max}} > X_{\mathrm{up}}$	352	5.2
$X_{\mathrm{up}} > 1080$ g/cm^2 or $dE/dX|_{X\mathrm{up}} > 150$ PeV/(g/cm^2)	0	0.0

TABLE I: Event-selection criteria and data-selection results. The number of events passing each selection criterion is reported, together with the corresponding fraction of events remaining, f.
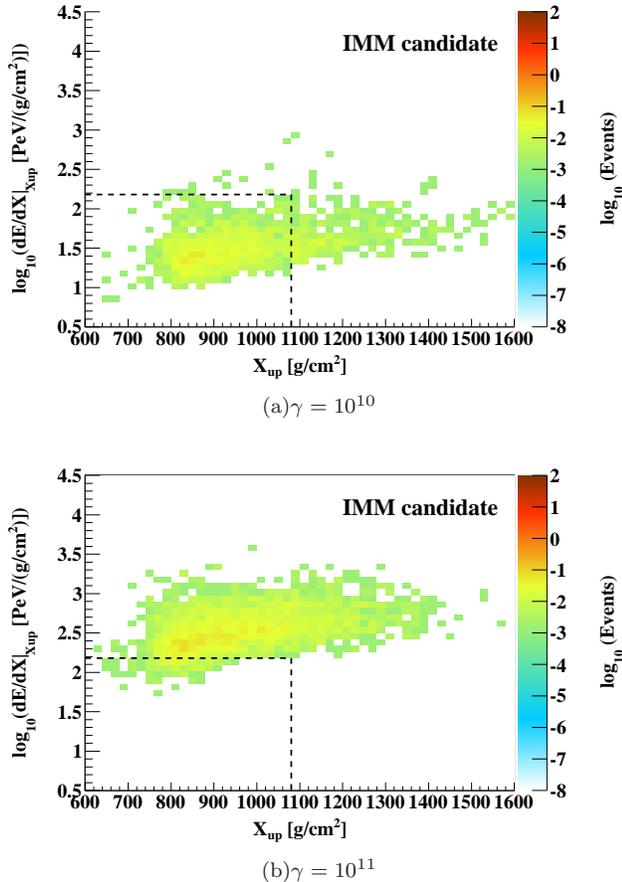
(a)$\gamma = 10^{10}$

(b)$\gamma = 10^{11}$

FIG. 5: Correlation of $dE/dX|_{X_{\rm up}}$ with $X_{\rm up}$ for simulated ultra-relativistic IMM of energy 10^{25} eV and Lorentz factors $\gamma = 10^{10}$(a) and 10^{11}(b). The color-coded scale indicates the number of events expected in the search-period data set assuming a flux of 10^{-20} (cm^2 sr s)$^{-1}$. Only events outside the dashed boxes are kept in the final selection for ultra-relativistic IMMs.

VI. EXPOSURE

The flux Φ of ultra-relativistic IMMs of Lorentz factor γ is given by

$$\Phi(\gamma) = \frac{k}{\mathcal{E}(\gamma)}, \tag{1}$$

where k is the number of events surviving the selection criteria of Table I (or an appropriate upper limit if no candidate is found), and $\mathcal{E}(\gamma)$ is the exposure, i.e., the time-integrated aperture for the hybrid detection of ultra-relativistic IMMs. The exposure is defined as [36]:

$$\mathcal{E}(\gamma) = \int_{S_{\rm gen}} \int_{\Omega} \int_{T} \epsilon(\gamma, t, \theta, \phi, x, y) \cos\theta dS d\Omega dt, \tag{2}$$

where ϵ is the detection efficiency for an ultra-relativistic IMM of zenith angle θ and azimuth angle ϕ intersecting

the ground at a position (x, y), Ω is the solid angle, $S_{\rm gen}$ is the area over which events are detectable, and T is the time period of the search data set.

In general, the detection efficiency ϵ changes over time, which must be taken into account in the calculation of the exposure. In fact, the effective area of the SD array and the number of operating FD telescopes grew during the Observatory installation from 2004 to 2008, and then varied due to occasional failures of the SD stations or FD telescopes. Sometimes weather conditions (e.g., wind, rain) introduced down-time in the operation of the FD. Also, the night-sky background and atmospheric conditions, such as aerosol concentration and cloud coverage, changed during data taking, which affected the sensitivity of the FD telescopes.

These effects were properly taken into account with a time-dependent detector simulation [36], which makes use of slow-control information and atmospheric measurements recorded during data taking. The detector configuration and atmospheric characteristics were changed in the simulation according to the time period T. For each Lorentz factor γ, we generated a number $N(\gamma, \cos\theta)$ of ultra-relativistic IMM showers over an area $S_{\rm gen}$, with $n(\gamma, \cos\theta)$ of them fulfilling the event-selection criteria of Table I. Then the exposure given by Equation 2 was numerically evaluated:

$$\mathcal{E}(\gamma) = 2\pi S_{\rm gen} T \sum_i \frac{n(\gamma, \cos\theta_i)}{N(\gamma, \cos\theta_i)} \cos\theta_i \Delta\cos\theta_i. \tag{3}$$

Table II shows the estimated hybrid exposure as a function of the IMM Lorentz factor. The exposure corresponding to the search period ranges from ≈ 100 km^2 sr yr for $\gamma = 10^9$ to ≈ 3000 km^2 sr yr for $\gamma \geq 10^{11}$. Several sources of systematic uncertainties were considered. The uncertainty of the on-time calculation resulted in an uncertainty of 4% on the exposure. The detection efficiency estimated through the time-dependent detector simulation depends on the fluorescence yield assumed in the simulation, on the FD shower-reconstruction methods and on the atmospheric parameters and FD calibration constants recorded during data taking. Following the procedures of [36], the corresponding uncertainty on the exposure was estimated to be 18%. To estimate the uncertainty associated with the event selection, we changed the size of the $(X_{\rm up}, dE/dX|_{X_{\rm up}})$ selection box according to the uncertainty on the two selection variables. $X_{\rm up}$ was changed by ± 10 g/cm^2, corresponding to the uncertainty on $X_{\rm max}$ [23], and $dE/dX|_{X_{\rm up}}$ was changed by the uncertainty on the FD energy scale [33]. The number of selected IMM events changed by 9%, which was taken as an estimate of the uncertainty on the exposure. From the sum in quadrature of these uncertainties, a total systematic uncertainty of 21% was assigned to the exposure.
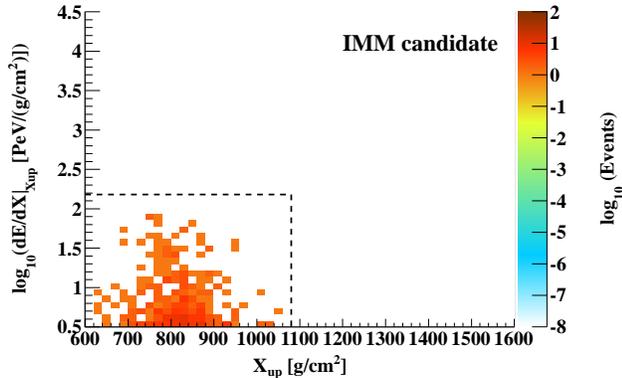
FIG. 6: Correlation of $dE/dX|_{X\text{up}}$ with X_{up} for the data sample passing the shower-quality selection criteria and $X_{\text{max}} > X_{\text{up}}$. The color-coded scale indicates the number of events. No event is found outside the dashed box in the final selection for ultra-relativistic IMMs.

VII. DATA ANALYSIS AND RESULTS

The search for ultra-relativistic IMMs was performed following a blind procedure. The selection criteria described in Section V were optimized using Monte Carlo simulations and a small fraction (10%) of the data. This training data set was excluded from the final search period. Then the selection was applied to the full sample of data collected between 1 December 2004 and 31 December 2012. The number of events passing each of the selection criteria is reported in Table I. The correlation of $dE/dX|_{X\text{up}}$ with X_{up} for events passing the shower-quality criteria and $X_{\text{max}} > X_{\text{up}}$ is shown in Figure 6. The corresponding distributions of $dE/dX|_{X\text{up}}$ and X_{up} are compared in Figure 7 with Monte Carlo expectations for a pure UHECR proton background, showing a reasonable agreement between data and simulations. The partial difference indicates there are heavier nuclei than protons as well. No event passed the final requirement in the $(X_{\text{up}}, dE/dX|_{X\text{up}})$ plane, and the search ended with no candidate for ultra-relativistic IMMs.

Given the null result of the search, a 90% C.L. upper limit on the flux of ultra-relativistic IMMs, $\Phi_{90\%\text{C.L.}}$, was derived from Equation 1, with exposure $\mathcal{E}(\gamma)$ as in Table II and $k = 2.44$. This value of k corresponds to the Feldman-Cousins upper limit [37] for zero candidates and zero background events. We derived in Section V a background level of 0.07 event which is likely to be overestimated, since a pure proton composition was assumed while heavier nuclei appear to be a dominant component at the highest energies [23]. In fact, the fraction of deeply-penetrating showers produced by heavy nuclei is significantly smaller resulting in fewer background events for the IMM search. Given the uncertainty in the background, we have taken a conservative approach and assumed zero background events, which provides a slightly
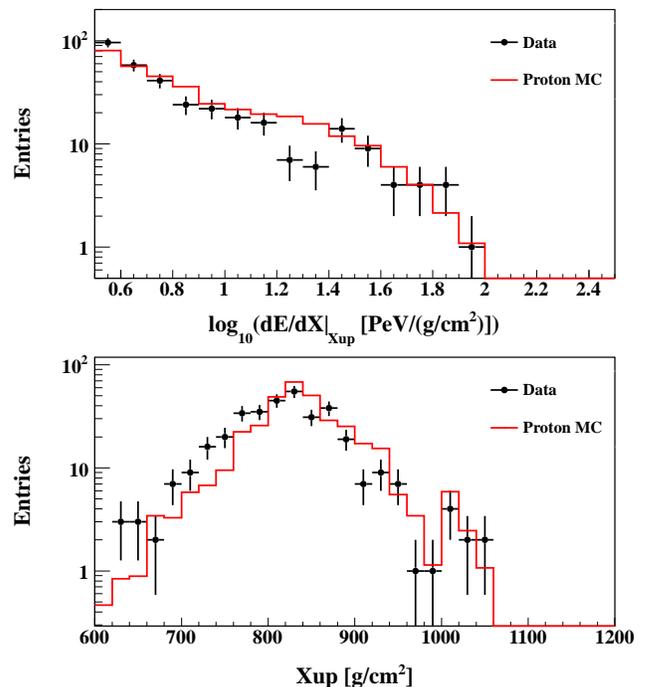
FIG. 7: Distribution of $dE/dX|_{X\text{up}}$ (a) and X_{up} (b) for the data sample (black dots) passing the shower-quality selection criteria and $X_{\text{max}} > X_{\text{up}}$. The red solid line is the Monte Carlo prediction for a pure UHECR proton background, normalized to the number of selected events in the data.

$\log_{10}(\gamma)$	$\mathcal{E}(\gamma)$ (km^2 sr yr)	$\Phi_{90\%\text{C.L.}}$ (cm^2 sr s)$^{-1}$
8	1.16	8.43 $\times 10^{-18}$
9	9.52 $\times 10^1$	1.03 $\times 10^{-19}$
10	4.50 $\times 10^2$	2.18 $\times 10^{-20}$
11	3.15 $\times 10^3$	3.12 $\times 10^{-21}$
≥ 12	3.91 $\times 10^3$	2.51 $\times 10^{-21}$

TABLE II: Exposure and 90% C.L. upper limits on the flux of ultra-relativistic IMMs ($E_{\text{mon}} = 10^{25}$ eV) for different Lorentz factors γ. A 21% Systematic uncertainty on the exposure was taken into account in the upper limits.

worse limit.

In Section VI we estimated a 21% systematic uncertainty on the exposure which must be taken into account in the upper limit. Rather than following the propagation of statistical and systematic uncertainties outlined in [38], which would worsen the upper limit by a factor of 1.05, we adopted a more conservative approach and multiplied $\Phi_{90\%\text{C.L.}}$ by a factor of $f = 1 + n \times 0.21$, where $n = 1.28$ corresponds to the 90% C.L.

Our final 90% C.L. upper limits on the flux of ultra-relativistic IMMs are reported in Table II and shown in Figure 8, together with results from previous experiments. Following the treatment of [13], the MACRO and SLIM limits extrapolated to $\gamma \geq 10^9$ were weakened by a factor of two to account for the IMM attenuation when passing through the Earth.
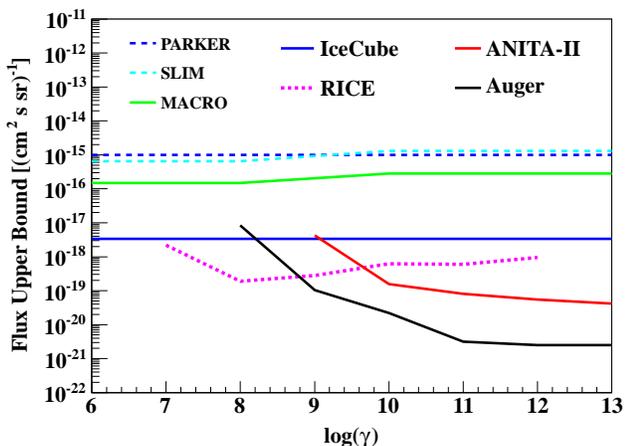
FIG. 8: 90% C.L. upper limits on the flux of ultra-relativistic IMMs: this work (black solid line); Parker bound (blue dashed line) [15]; SLIM (sky-blue dashed line) [11], MACRO (green solid line) [8], IceCube (blue solid line) [14], RICE (pink dotted line) [12] and ANITA-II (red line) [13]. The MACRO and SLIM limits above $\gamma = 10^9$ were weakened by a factor of two to account for the IMM attenuation through the Earth.

Several checks of the analysis were performed. Variation of the selection criteria within reasonable ranges still resulted in no candidate. The UHECR energy spectrum was varied within its uncertainties [33], with negligible effect on the background estimation. The background for the IMM search is dominated by deeply-penetrating UHECR showers, which are found in the tail of the $X_{\max}$ distribution and depend on the characteristics of the hadronic interactions. We used three different hadronic-interaction models (Section V) to simulate UHECR protons for background estimation. Ultrahigh-energy photons are also expected to produce deeply-penetrating showers, which may mimic an IMM event. The photon hypothesis should be carefully evaluated in case a candidate IMM is found. Since this search ended with a null result, the zero background assumption produces the most conservative limit also including the possibility of ultrahigh-energy photons. Lastly, we compared the CORSIKA energy-loss model with analytical approximations and other Monte Carlo codes [39], and found good agreement.

VIII.   CONCLUSIONS

We presented the first search for magnetic monopoles ever performed with a UHECR detector, using the Pierre Auger Observatory.   The particle showers produced by electromagnetic interactions of an ultra-relativistic monopole along its path through the atmosphere result in an energy deposit comparable to that of a UHECR, but with a very distinct profile which can be distinguished by the fluorescence detector. We have looked for such showers in the sample of hybrid events collected with Auger between 2004 and 2012, and no candidate was found. A 90% C.L. upper limit on the flux of magnetic monopoles was placed, which is compared with results from previous experiments in Figure 8. Ours is the best limit for $\gamma \geq 10^9$, with a factor of ten improvement for $\gamma \geq 10^{9.5}$. This result is valid for a broad class of intermediate-mass ultra-relativistic monopoles ($E_{\mathrm{mon}} \approx 10^{25}$ eV and $M \sim 10^{11} - 10^{16}$ eV/c^2) which may be present today as a relic of phase transitions in the early universe. Since the background - less than 0.1 event in the current data set - is not a limiting factor in the search, the upper bound will improve with the steadily increasing exposure of the Pierre Auger Observatory.

[1] P. A. Dirac, Proc. Roy. Soc. Lond. **A133**, 60 (1931).
[2] J. Preskill, Ann. Rev. Nucl. Part. Sci. **34**, 461 (1984).
[3] G. Giacomelli, Riv. Nuovo Cim. **7**, 1 (1984).
[4] D. E. Groom, Phys. Rept. **140**, 323 (1986).
[5] T. W. Kephart and T. J. Weiler, Astropart. Phys. **4**, 271 (1996), astro-ph/9505134.
[6] C. Escobar and R. Vazquez, Astropart. Phys. **10**, 197 (1999), astro-ph/9709148.
[7] S. D. Wick, T. W. Kephart, T. J. Weiler, and P. L. Biermann, Astropart. Phys. **18**, 663 (2003), astro-ph/0001233.
[8] M. Ambrosio et al. (MACRO Collaboration), Eur. Phys. J. **C25**, 511 (2002), hep-ex/0207020.
[9] H. Wissing (IceCube Collaboration), Proc. of the 30th International Cosmic Ray Conference, Merida, Mexico (2007).
[10] V. Aynutdinov et al. (Baikal Collaboration), Proc. of the 29th International Cosmic Ray Conference, Pune, India (2005), astro-ph/0507713.
[11] S. Balestra et al., Eur. Phys. J. **C55**, 57 (2008), 0801.4913.
[12] D. Hogan, D. Besson, J. Ralston, I. Kravchenko, and D. Seckel, Phys. Rev. **D78**, 075031 (2008), 0806.2129.
[13] M. Detrixhe et al. (ANITA-II Collaboration), Phys. Rev. **D83**, 023513 (2011), 1008.1282.
[14] R. Abbasi et al. (IceCube Collaboration), Phys. Rev. **D87**, 022001 (2013), 1208.4861.
[15] E. N. Parker, Astrophys. J. **160**, 383 (1970).
[16] F. C. Adams et al., Phys. Rev. Lett. **70**, 2511 (1993).
[17] A. Aab et al. (Pierre Auger Collaboration), Nucl. Instrum. Meth. **A798**, 172 (2015), 1502.01323.
[18] I. Allekotte et al. (Pierre Auger Collaboration), Nucl. Instrum. Meth. **A586**, 409 (2008), 0712.2832.
[19] J. Abraham et al. (Pierre Auger Collaboration), Nucl. Instrum. Meth. **A620**, 227 (2010), 0907.4282.
[20] J. Rosado, F. Blanco, and F. Arqueros, Astropart. Phys. **55**, 51 (2014), 1401.4310.
[21] M. Ave et al. (AIRFLY Collaboration), Astropart.Phys. **42**, 90 (2013), 1210.6734.
[22] M. Ave et al. (AIRFLY Collaboration), Astropart.Phys. **28**, 41 (2007), astro-ph/0703132.
[23] A. Aab et al. (Pierre Auger Collaboration), Phys. Rev. **D90**, 122005 (2014), 1409.4809.
[24] V. Verzi et al. (Pierre Auger Collaboration), Proc. of the 33rd International Cosmic Ray Conference, Rio de Janeiro, Brazil (2013), 1307.5059.
[25] S. P. Ahlen, Rev. Mod. Phys. **52**, 121 (1980).
[26] D. Heck, G. Schatz, T. Thouw, J. Knapp, and J. Capdevielle, Forschungszentrum Karlsruhe Report FZKA p. 6019 (1998).
[27] T. Bergmann et al., Astropart. Phys. **26**, 420 (2007), astro-ph/0606564.
[28] S. R. Kelner and Y. D. Kotov, Sov. J. Nucl. Phys. **7**, 237 (1968).
[29] R. P. Kokoulin and A. A. Petrukhin, Proc. of the 12th International Cosmic Ray Conference, Hobart, Australia **6**, A 2436 (1971).
[30] L. B. Bezrukov and E. V. Bugaev, Sov. J. Nucl. Phys. **5**, 33 (1981).
[31] E. V. Bugaev and Y. V. Shlepin, Phys. Rev. **D67**, 034027 (2003).
[32] H. Abramowicz and A. Levy (1997), hep-ph/9712415.
[33] A. Schulz et al. (Pierre Auger Collaboration), Proc. of the 33rd International Cosmic Ray Conference, Rio de Janeiro, Brazil (2013), 1307.5059.
[34] S. Argiro et al., Nucl. Instrum. Meth. **A580**, 1485 (2007), 0707.1652.
[35] T. K. Gaisser and A. M. Hillas, Proc. of the 15th International Cosmic Ray Conference, Plovdiv, Bulgaria **8**, 353 (1977).

[36] P. Abreu et al. (Pierre Auger Collaboration), Astropart. Phys. **34**, 368 (2011), 1010.6162.

[37] G. J. Feldman and R. D. Cousins, Phys. Rev. **D57**, 3873 (1998), physics/9711021.

[38] R. D. Cousins and V. L. Highland, Nucl. Instrum. Meth. **A320**, 331 (1992).

[39] D. Chirkin and W. Rhode (2004), hep-ph/0407075.